A study of convective heat transfer and phase changes in subglacial liquid environment

Clément de la Salle
supervisor: Louis-Alexandre Couston

May to July 2021

Table des matières

Introduction

The presence of sub-glacial water pocket, and oceans, on some moons of the solar system is today highly suspected [1]. The study of the distribution, the dynamic, the scales involved of those reservoirs is crucial to interpret the satellite data and guide the future exploration mission, to determine the habitability of the solar system [2].

The existence of such water pocket, has only recently been proposed to explain the presence of brine deposit, and some little scale topography on the surface of Enceladus for example [3]. The researches about the formation mechanisms of those liquid cavity under the ice are still a in infancy, and generally suppose a partial melting due to tidal heating. [4].

Newer studies, focusing on the collapse of such pockets in order to clarify the presence of the topography on surface via the ascent of the initially subglacial water, use an empiric uniform and isotropic model for the heat transfer between liquid and solid [5]. This must be highly approximated to describe the flow inside the cavity, since it imposes an arbitrary longevity and a self-similar geometry. For such system, we expect in particular the disk geometry to be broken : with a positive thermal expansion coefficient, the upper half should be unstable and turbulent, while the lower half must be stratified. This implies a strong asymmetry of heat transfers between the top (where the heat convection is dominant) and the bottom of the reservoir, which completely breaks with the auto-similar assumption. So this will have a crucial impact on the final results, in particular on the longevity of the the cavity, and thus, on the cryomagma ascent eruptions previously studied.

Also, some other studies have already been led on the turbulence in a disk geometry [6] [7], but the boundary conditions where completely different, considering different fixed temperature at the top and the bottom of it. Here we want the liquid to be at a constant melting temperature along its whole border. The main difference is that cold top and warm bottom boundary conditions can't lead to a global cooling of the system, which quite a crucial phenomenon for our problem. Still those papers can help us to get some clue on the turbulence in such a geometry, and to define useful quantities. We also want to go further by introducing the phase change. The coupling between turbulence and phase change also already have been studied [8], but still with other boundary conditions, where the global temperature remains constant.

In this internship, we propose to push forward the knowledge of those water pockets under glacial environment, thanks to numerical simulations of the flow at moderate pressure and temperature, together with some phase changes. In order to have precise but still fast simulations, we will use the phase field method [9]. We will solve the spatial heterogeneity, so that we can observe the exact form of the cavity in function of time, seeing it grow in a first instance, then shrink when the water become sufficiently cold. We propose here to take initial steps toward a model in order to answer the following questions :

i) How does the flow look like in the water pocket ? In particular, what type of turbulence can we find in it ?

ii) How does the shape of the pocket evolve in time and what are the typical temporal scales ? Introducing the possibility of phase change, shall we see the water disappear, move in space ?

The main goal of the internship is to start some numerical simulations to find answers to those questions. We will only consider 2D flows, since this is the very beginning of such study, so there is no need to implement heavy simulations that require too much time and data storage.

The code we are using to compute our simulations is `dedalus` [10], since the efficiency of this open-source and pseudo-spectral code, in phase change studies and in presence of a turbulent flow, has recently been proven [8].

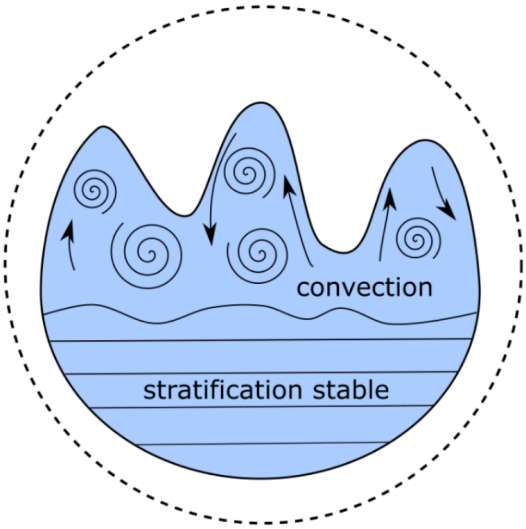

FIGURE 1 – We expect the convection to be effective in the upper part of the cavity, where the cold boundary is upward the hot fluid, whereas we have the opposite situation in the lower part where the temperature is then expected to be stratified. Moreover, the geometry will evolve during time.

1 RAYLEIGH-BÉNARD convection

The first step is to learn about `dedalus`, and try to implement a simple problem, widely documented : the RAYLEIGH-BÉNARD convection. This first part of the internship has for the following goals :

1. To learn how to use `dedalus` and run our first simulations on the supercomputer PSMN
2. To familiarize ourselves with the physical control parameters and how they influence the dynamic...
3. But also with the numerical parameters (time and spatial steps, needed resources in time and size)
4. To understand the first turbulence mechanisms, that we can find in the final system

1.1 Presentation of the problem

1.1.1 Physical problem and equations

We consider a fluid in a 2-dimensional box (length L and height h) with gravity along the vertical axis. We impose a fixed temperature $+\Delta T/2 > 0$ at the bottom and $-\Delta T/2$ at the top. We suppose that the density of the fluid follows a linear evolution with the temperature :

$$\rho = \rho_0(1 - \beta(T - T_0)) = \rho_0 + \delta\rho \qquad \text{with} \quad \rho_0 = \rho(T_0)$$

Where T_0 is a given reference temperature. The lighter hot fluid undergo a force that makes it buoyant, when the cold one at the top is attracted to the bottom. Thus, we can see an instability : the RAYLEIGH-BÉNARD instability.

To quantitatively understand the problem, we start to give its equations 1.1. We make the BOUSSINESQ approximation ($|\delta\rho| \ll \rho_0$), which leads to keep the density variations only in the gravitational term, of the NAVIER-STOCKES equations :

$$\begin{cases} \rho_0 \left(\dfrac{\partial \boldsymbol{u}}{\partial t} + \boldsymbol{u} \cdot \boldsymbol{\nabla} \boldsymbol{u} \right) = -\boldsymbol{\nabla} P + \delta\rho\, \boldsymbol{g} + \nu \rho_0 \nabla^2 \boldsymbol{u} \\ \boldsymbol{\nabla} \cdot \boldsymbol{u} = 0 \\ \dfrac{\partial T}{\partial t} + \boldsymbol{u} \cdot \boldsymbol{\nabla} T = \kappa \nabla^2 T \end{cases} \tag{1.1}$$

1.1.2 Non-dimensionalisation

The problem involves many parameters : the reference density ρ_0, the intensity of the gravitational field g, the kinematic viscosity ν, the thermal diffusivity κ, the difference of temperature imposed at the boundaries ΔT, the size of the box L and h. To reduce the dimensions of the problem, it is useful to non-dimensionalize those quantities :

$$\tilde{x} = \frac{x}{h} \qquad \tilde{t} = \frac{\kappa}{h^2}\, t \qquad \tilde{P} = \frac{h^2}{\rho_0 \kappa^2}\, P$$
$$\tilde{z} = \frac{z}{h} \qquad \tilde{\boldsymbol{u}} = \frac{h}{\kappa}\, \boldsymbol{u} = \begin{pmatrix} \tilde{u} \\ \tilde{w} \end{pmatrix} \qquad \tilde{T} = \frac{T - T_{lin}}{\Delta T}$$

Were T_{lin} is the purely diffusive solution of the problem (without gravity, nor convection) :

$$T_{lin} = -\frac{\Delta T}{h}\, z = -\Delta T\, \tilde{z}$$

Thus, the non-dimensional equations, only involve two control parameters (cf. Appendix) :

$$\begin{cases} \dfrac{1}{\mathrm{Pr}} \left(\dfrac{\partial \tilde{\boldsymbol{u}}}{\partial \tilde{t}} + \tilde{\boldsymbol{u}} \cdot \tilde{\boldsymbol{\nabla}} \tilde{\boldsymbol{u}} \right) = -\tilde{\boldsymbol{\nabla}} \tilde{p} + \mathrm{Ra}\, \tilde{T}\, \boldsymbol{e_z} + \tilde{\nabla}^2 \tilde{\boldsymbol{u}} \\ \tilde{\boldsymbol{\nabla}} \cdot \tilde{\boldsymbol{u}} = 0 \\ \dfrac{\partial \tilde{T}}{\partial \tilde{t}} + \tilde{\boldsymbol{u}} \cdot \tilde{\boldsymbol{\nabla}} \tilde{T} - \tilde{w} = \tilde{\nabla}^2 \tilde{T} \end{cases}$$

With the Rayleigh and Prandlt numbers respectively

$$\mathrm{Ra} = \frac{\rho_0 h^3 \beta\, \Delta T}{\kappa \nu} \qquad \mathrm{Pr} = \frac{\nu}{\kappa}$$

Qualitatively, we understand that Ra acts as an external forcing (in particular it is proportional to ΔT) and Pr as the comparison of the viscous and thermal diffusivities. Until the end of the internship, we will only consider $\mathrm{Pr} = 1$, that is to say the scales (time and space) are the same for both types of diffusivity.

In addition of those two non-dimensional numbers, there is a third one (independent) : the aspect ratio

$$\gamma = \frac{L}{h}$$

We will always keep $\gamma = 4$ in our simulations, i.e. which is relatively large to minimize lateral confinement effects on the convective cells.

From now, we forgot the notation $\tilde{.}$ and all the fields are considered non-dimensional. The only physical parameter that we will study is Ra.

1.1.3 Boundary conditions

The boundary conditions that we fix are the following :

Speed No-slip condition at the top and at the bottom : $\boldsymbol{u}(z=0) = \boldsymbol{u}(z=h) = \boldsymbol{0}$

Temperature Fixed temperature on each border : $T(z=0) = -\Delta T/2$, $T(z=h) = +\Delta T/2$

Moreover, since `dedalus` uses pseudo-spectral methods, at the most one dimension can be non-periodic, here the vertical one. So we now have another boundary condition : all the fields must be periodic along the horizontal axis.

1.2 Physical context

1.2.1 Other non-dimensional numbers

As we just discussed before, the input of the system is fully determined by the RAYLEIGH number. But we can define other non-dimensional numbers to study the response of the system for a given Ra :

— Of course the REYNOLDS number, which is defined as follows (function of the non-dimensional fields and numbers) :

$$\mathrm{Re} = \frac{U_{rms}}{\mathrm{Pr}} \qquad \text{with} \quad U_{rms} = \sqrt{u^2 + w^2}$$

This number allows us to quantify the turbulence.

— The second aspect of the problem is the heat transfers. To study them, we define the NUSSELT number :

$$\mathrm{Nu} = \frac{q}{q^{lin}}$$

This number, compares the vertical total heat flux q with the flux in the purely diffusive regime q^{lin} (where $T = -z$ and $\boldsymbol{u} = \boldsymbol{0}$), we show (cf. APPENDIX) that it can be rewritten as follows :

$$\mathrm{Nu} = q_{diff} + q_{conv} \qquad \text{with} \quad q_{diff} = 1 - \partial_z T \quad \text{and} \quad q_{conv} = Tw$$

1.2.2 Different types of mean

In order to study the properties of the flow, we'll need to compute some fields averages. Here we have three different possible choices, because there are three independent dimensions (1 in time, 2 in space). Let X be a given field, we can define :

Temporal average	Horizontal average	Vertical average
$\bar{X}(x,z) = \dfrac{1}{t_f - t_i}\displaystyle\int_{t_i}^{t_f} X \,\mathrm{d}t$	$\langle X\rangle_x(t,z) = \dfrac{1}{\gamma}\displaystyle\int_0^{\gamma} X \,\mathrm{d}x$	$\langle X\rangle_z(t,x) = \displaystyle\int_0^{1} X \,\mathrm{d}z$

By combination of the two space averages, we can get the volume mean :

$$\langle X\rangle_V(t) = \langle\langle X\rangle_x\rangle_z = \langle\langle X\rangle_z\rangle_x$$

From those definitions, we can derive some important properties, particularly simplifications for the expression of Nu (cf. APPENDIX) :

$$\begin{aligned} \langle \mathrm{Nu} \rangle_x(t,z) &= 1 + \langle Tw \rangle_x - \langle \partial_z T \rangle_x \\ \langle \mathrm{Nu} \rangle_V(t) &= 1 + \langle Tw \rangle_V \\ \langle \overline{\mathrm{Nu}} \rangle_x(z) &= \text{cste} \end{aligned} \tag{1.2}$$

1.3 Numerical Context

For the purpose of numerically solving the problem, we control two parameters : the spatial and the temporal resolution. The first one is simply determined by the number of nodes along each axis :

Horizontal axis We use a periodic base, since the problem itself is periodic along this axis. Let n_x be the number of nodes along x.

Vertical axis Here we use a Chebyshev base, tighter on the boundaries, in order to have a better resolution of the small diffusive boundary layers. For an aspect ratio $\gamma = 4$, we will keep the number of nodes along the vertical axis $n_z = n_x/2$ (cf. Figure 1.1)

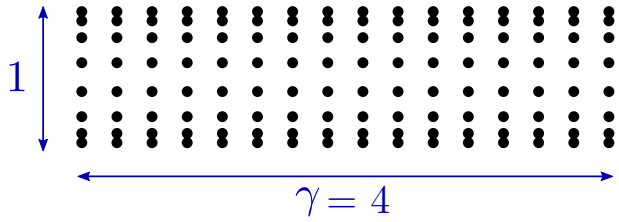

Figure 1.1 – Appearance of the spatial decomposition for $n_x = 2n_z = 16$ with $\gamma = 4$. The base is periodic along the horizontal axis and we use a Chebysheb one for the vertical axis.

Considering the temporal resolution, `dedalus` includes an automatic computation of the time step, in function of the intensity of the flow (the Reynlods number) and a numerical parameter called `safety`. The smaller it is, the higher the resolution will be.

So finally, on we will only control two numerical parameters : the numer of nodes along the horizontal axis n_x (which fixes $n_z = n_x/2$) and the `safety` for the time scale. Of course, the values we choose for those parameters highly depends on the physical ones (that is to say Ra). For instance, we can study the needed resolution n_x in function on Ra... The ratio between the greatest length scale L and the smallest one (the Kolmogorov length microscale η) evolves like

$$\frac{L}{\eta} \propto \mathrm{Re}^{3/4}$$

In an other hand, the resolution n_x must be sufficiently high to solve the smallest scale : $n_x \propto \eta^{-1}$. Then we use an empirical law, that we discuss in the sub-section 1.4.1 : $\mathrm{Re} \propto \mathrm{Ra}^{1/2}$, so that we finally get

$$n_x \propto \mathrm{Ra}^{3/8}$$

In particular, if we multiply Ra by in order of 10, we should increase the resolution by a factor of $10^{3/8} \sim 2$.

1.4 Results

1.4.1 Physical considerations

Let's start with the verification of the shape of the flow. On Figure 1.2, we plot the appearance of some fields at two different times : during the transition and the permanent (statistically steady)

regime. We can clearly see (thanks to the speed fields u and w) the shape of the expected convection cells. They can also been observed on the temperature field...

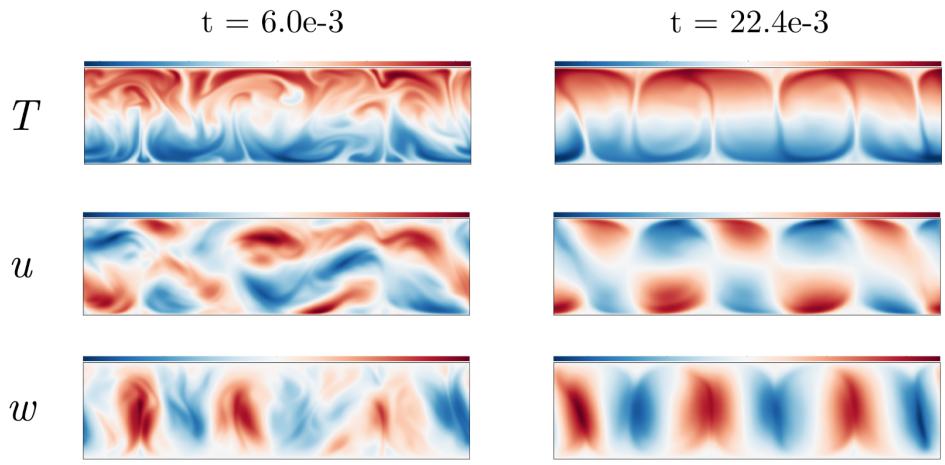

FIGURE 1.2 – Examples of the shape of some fields. The RAYLEIGH number has been chosen at $\mathrm{Ra} = 10^6$. We see the establishment of the final convection cells, through the transition regime.

One of the objectives of this study, is to focus on the non-dimensional numbers Re and Nu. But before we dive into their dependence with Ra, we can start by observing their behaviour in time and space. For the sake of clarity, we will always compute their x-average. On FIGURE 1.3, we can see the different mean of those numbers Nu and Re. We can do the following observations :

— There is a transition regime, after which the system has a permanent cyclic evolution. On this permanent regime, the non-dimensional numbers have a stationary behaviour, the final totale average (in time and space) should be computed only in this regime.

— On the profiles $\langle \bar{X} \rangle_x(z)$, we observe that $\langle \overline{\mathrm{Nu}} \rangle_x(z) \sim \mathrm{cste}$, which is coherent with the theory (cf. APPENDIX). Also, we see that $\langle \overline{\mathrm{Re}} \rangle_x(z)$ vanishes on the border (because of the no-slip condition) and is maximal in an intermediary zone, between the bulk and the boundary layer. Indeed, the fluid is "crushed" on the wall because of the convection cells, so it has to have a higher speed, since it is incompressible.

— For the spatial averages $\langle X \rangle_V(t)$, each number oscillates during the permanent regime, around a mean value. This is the value that interest us and the only one we will associate to a given simulation $\langle \bar{X} \rangle_V \in \mathbb{R}$.

Now, we know how to associate a single value of Nu and Re to one simulation (that is to say, to one given Ra). We find in the literature that both of the number Nu and Re are linked to Ra in such a system, with power laws. It is a bit hard to extract one reference law, since there is no consensus and they can vary from a paper to an other... Still for the NUSSELT number, we often find the following propositions : $\mathrm{Nu} \sim \mathrm{Ra}^{1/3}$ for $\mathrm{Ra} \geq 10^{11}$ [11] or $\mathrm{Nu} \sim \mathrm{Ra}^{2/7}$ [12]. In their unifying theory [11], GROSSMAN and LOHSE points out that the scaling law hardly depends on the domain in the Ra/Pr plane. Considering our simulations, where $\mathrm{Pr} = 1$ and $\mathrm{Ra} \leq 10^{10}$, we will keep in mind the theoretical proposition of that last paper :

$$\mathrm{Nu} \sim \mathrm{Ra}^{1/4} \qquad \mathrm{Re} \sim \mathrm{Ra}^{1/2}$$

Note that those results only apply for turbulent flows, so we can expect to have slightly different values, since we will also considered non- or moderately-turbulent flows.

We see on FIGURE 1.4 the expected scaling law for Nu. The one for Re differs of around 10% (0.55 instead of 0.5). This first result will not be subject of a further study, it mainly forms an intermediary step to check the coherence of the physical results.

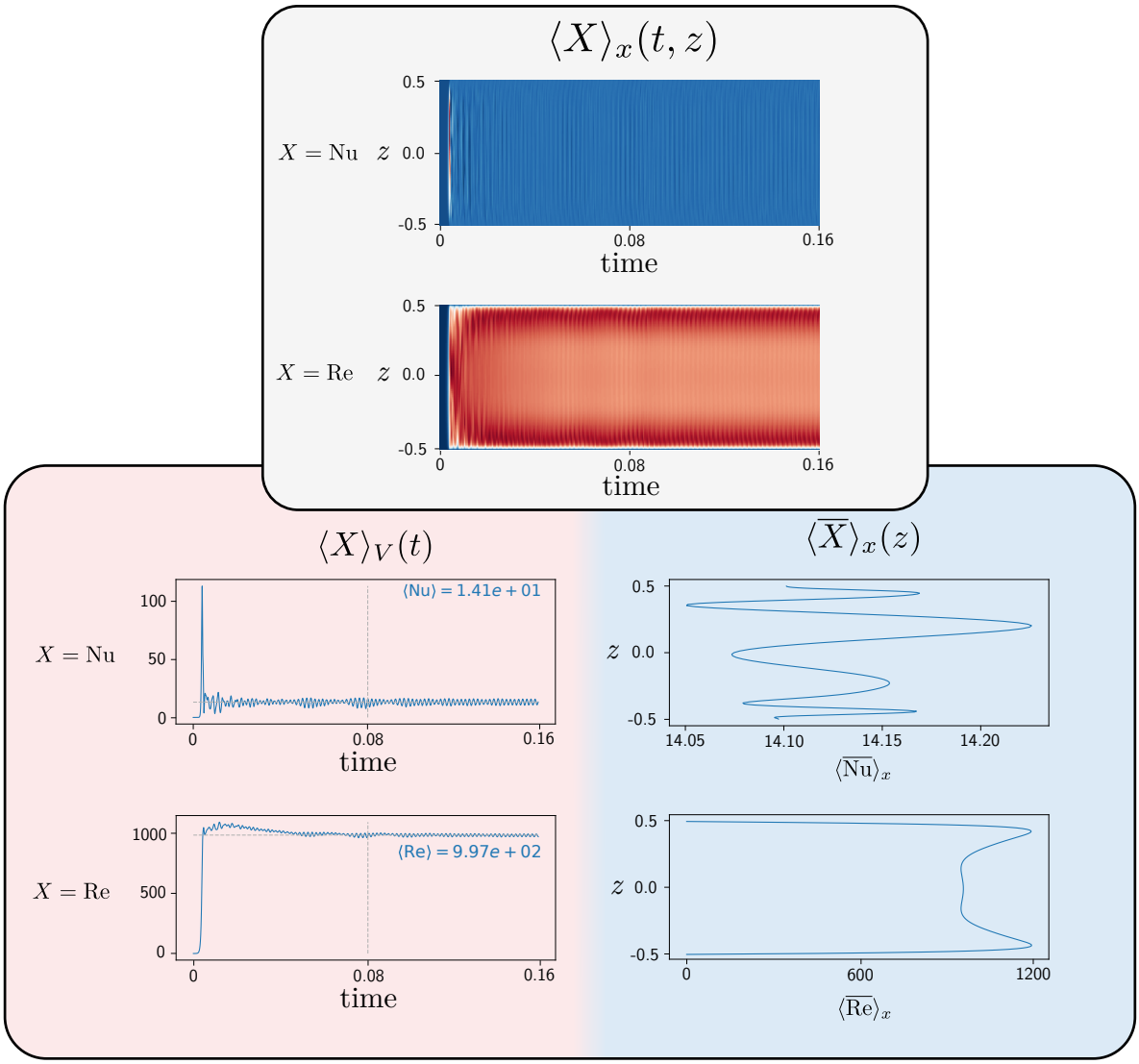

FIGURE 1.3 – Different types of mean for a simulation at $\mathrm{Ra} = 10^7$. For the volume average in function of time, the vertical dotted line represent the time at which we start to compute the time-averaged value, displayed on the graph.

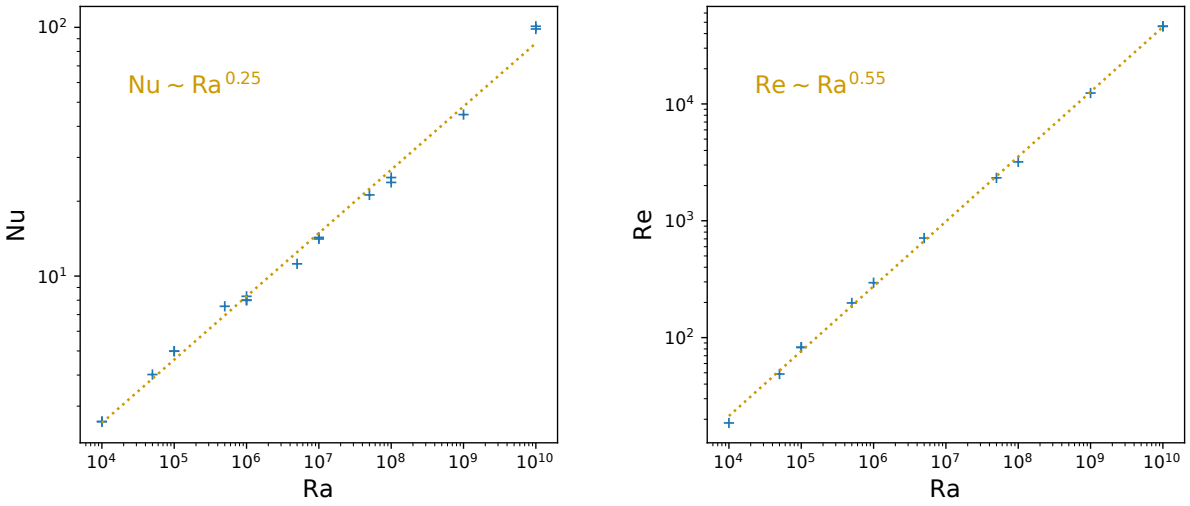

FIGURE 1.4 – Evolution of Nu and Re in function of Ra. We can find the scaling laws, of $\mathrm{Nu} \sim \mathrm{Ra}^{1/4}$ et $\mathrm{Re} \sim \mathrm{Ra}^{1/2}$

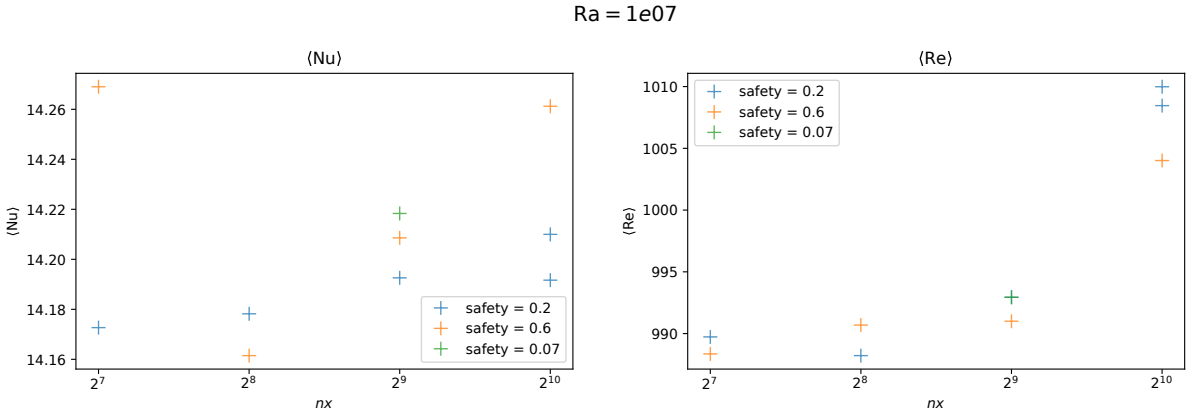

FIGURE 1.5 – Convergence of the final values, calculated for different numerical parameters n_x and `safety` for RAYLEIGH number $\mathrm{Ra} = 10^7$.

1.4.2 Numerical considerations

Now we try to investigate how these physical results are modified if we change some numerical parameters. As explained before, we will focus on the impact of the resolution n_x (n_z fixed to $n_z = 2n_x$) and the `safety`, that controls the temporal increment. The FIGURE 1.5 shows the influence of that variables on the final results $\langle \overline{\mathrm{Nu}} \rangle_V$ and $\langle \overline{\mathrm{Re}} \rangle_V$. The relative variations in both case are less than 1%, so we can consider it as negligible. The `safety` $= 0.07$ doesn't seems to bring much precision, so we will keep `safety` $= 0.2$ by now.

As seen before, we must double the resolution n_x when Ra is multiplied by 10. Given that consideration, we can predict the resolution needed for the next simulations :

Ra	n_x
...	...
10^5	32
10^6	64
10^7	128
10^8	256
...	...

TABLE 1 – Resolution in function of the RAYLEIGH number.

2 Inclusion of phase changes

To go deeper to the final system, we still consider the convection in a fluid band, but now we add a solid layer at the top of it. We should now take into account that the water can freeze at the interface, as well as the solid can melt. To implement this, we will use the phase field method [9].

2.1 Phase-field method

In this method,we keep our equations but add a new field : the **phase-field** ϕ. This field takes values between 0 (solid) and 1 (liquid). There is a zone (called the **damping zone**), where this field moves from 0 to 1 on a thickness 2δ. This parameter should be as small as possible (since the real physic interface is only a line), but cannot go under a certain limit, because the spectral method requires only continuous field. There is then a happy medium to choose this thickness δ, we typically take $\delta = 2\,\mathrm{d}z$ where $\mathrm{d}z$ is the local spatial vertical increment.

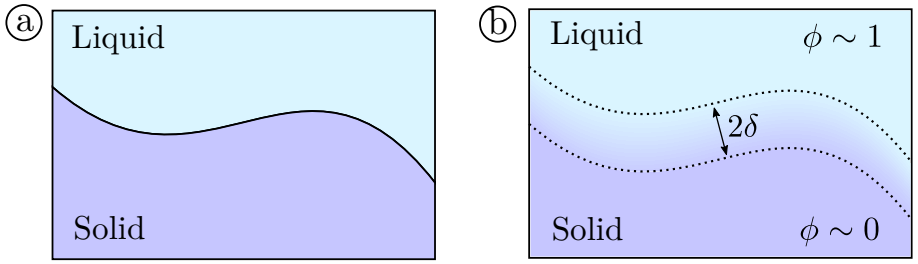

FIGURE 2.1 – The physical system (a) is composed of two phases, separated by a 1-dimensional interface. In the phase-field method (b), the phase becomes a continuous field, that varies between 0 and 1 on a damping zone of thickness 2δ

The equations will be modified as follows :

$$\begin{cases} \operatorname{div} \boldsymbol{u} = 0 \\ \partial_t \boldsymbol{u} + \boldsymbol{u} \cdot \boldsymbol{\nabla} \boldsymbol{u} = \mathrm{Pr}\, \nabla^2 \boldsymbol{u} - \boldsymbol{\nabla} p + \mathrm{Ra}\, \mathrm{Pr}\, T\, \boldsymbol{e_z} - \dfrac{\mathrm{Pr}}{\Gamma}(1-\phi)\,\boldsymbol{u} \\ \partial_t T + \boldsymbol{u} \cdot \boldsymbol{\nabla} T = \nabla^2 T - \mathrm{St}\, \partial_t \phi \\ \dfrac{5}{6}\mathrm{St}\, \partial_t \phi = \nabla^2 \phi + \dfrac{16}{\delta^2}\, \phi(1-\phi)(2\phi - 1 + T) \end{cases} \tag{2.1}$$

The NAVIER-STOCKES equation has a new term that vanishes in the fluid ($\phi = 1$), so it will only act as a damping term is the solid. This is the way we mimic the no-slip condition. The heat equation also gets a new term proportional to the variation of phase $\partial_t \phi$, it represents the heat that can be consumed/produced during the melting/solidification. Finally we get a whole new equation that describes the evolution of the phase-field. The form and the parameters has been optimized, so that the damping zone remain smaller than every physical length scale at anytime, and of course such that the system convergence to the real solution (a). There is a more precise discussion of the last term $\phi(1-\phi)(2\phi - 1 + T)$ in the APPENDIX 4.3

There is also three new parameters compared to the classical RAYLEIGH-BÉNARD case :

St The STEFAN number is a new dimensionless number that compares the latent heat $\mathcal{L}$ with the potential heat :

$$\mathrm{St} = \frac{\mathcal{L}}{c_p \Delta T}$$

This is a physical parameter, that has to be fixed as well as Pr and Ra to get a single solution of the problem.

Γ This one only shows up in the damping term so is a non-physical parameter. It controls the force of the damping and always has to be bigger than $2\mathrm{d}t$ where $\mathrm{d}t$ is a time step. We will take $\Gamma = 2\mathrm{d}t_{max}$ here.

δ This is related to the initial damping zone thickness and appears in this equation to provide this thickness

2.2 Convergence to the real solution

Of course this method is purely artificial and the phase field doesn't exist in experiments. The real solution must be calculated, using two different domains with their own set of equations and considering the dynamic of their interface. This method is designed so that it is equivalent when $\delta \to 0$, and its big advantage is its time demand, which is really low compared to the exact computation. That's why before trying to implement any physical solution, we tried to investigate the influence of the new terms, to verify the coherence of the results.

The idea is to study the same system as before (on the rectangular geometry), imposing a temperature difference on each side. Before, the boundary conditions were verified thanks to `dedalus`. Here we put a solid layer over the liquid, so we need to find an other way to fix the temperature **at the top of the fluid** (at the interface). The idea is to reuse the penalization method : to verify the no-slip condition, we put a damping term proportional to $(1-\phi)\,\boldsymbol{u}$ in the NAVIER-STOCKES equation... We do the same for the heat equation, so that the temperature is damped to zero in the solid, so we replace the phase change term to a damping one and we remove the phase evolution equation, since we wan't to compare the system with the previous (static) one.

$$\begin{cases} \operatorname{div} \boldsymbol{u} = 0 \\ \partial_t \boldsymbol{u} + \boldsymbol{u} \cdot \boldsymbol{\nabla} \boldsymbol{u} = \mathrm{Pr}\, \nabla^2 \boldsymbol{u} - \boldsymbol{\nabla} p + \mathrm{Ra}\, \mathrm{Pr}\, T\, \boldsymbol{e_z} - \dfrac{\mathrm{Pr}}{\Gamma}(1-\phi)\,\boldsymbol{u} \\ \partial_t T + \boldsymbol{u} \cdot \boldsymbol{\nabla} T = \nabla^2 T - \dfrac{\mathrm{Pr}}{\Gamma}(1-\phi)\,T \end{cases} \tag{2.2}$$

They are the same as equations 2.1, except we removed the equation of evolution of ϕ, so that the solid phase keep its initial geometry. We also changed the term of phase change $\mathrm{St}\partial_t \phi$ for a damping one $-\frac{\mathrm{Pr}}{\Gamma}(1-\phi)\,T$. This is the way we keep the temperature to zero everywhere in the solid (in particular on the interface). Instead of going in the phase change, the energy will artificially leave the disk in this well of energy.

With that new set of equation, we can impose with `dedalus` a bottom temperature, so that we have the exact same problem as before :

— Rectangular geometry (with the same aspect ratio γ)

— Bottom (resp. top) temperature fixed to hot (resp. cold)

— No-slip condition at the bottom and the top

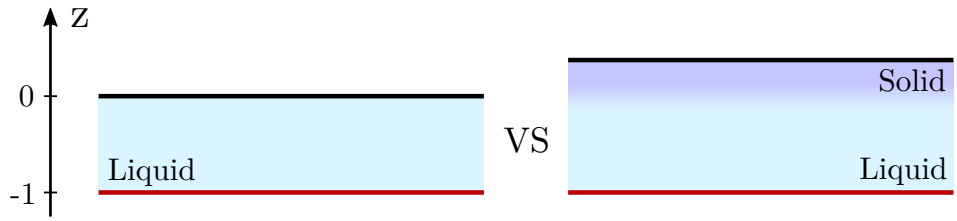

FIGURE 2.2 – In the first case, all boundary conditions are fixed by `dedalus`. In the second one, the top boundary conditions are verified thanks to the damping terms, that make the speed and the temperature vanish at the interface.

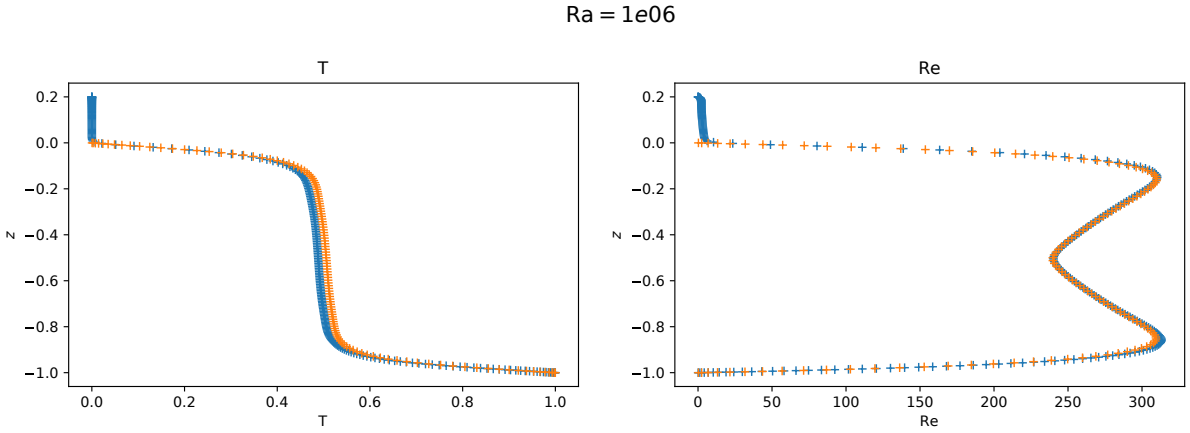

FIGURE 2.3 – Average profiles (along x and time) of the temperature (left) and the REYNOLDS number (right) in the real RAYLEIGH-BÉNARD problem (orange) and the damped problem (blue).

But as shown on the FIGURE 2.2, the way we check the top boundary conditions is different. The goal is to verify that this penalization method won't have any impact on our results.

On FIGURE 2.3, the average profiles of T and Re are very close to each other. In particular the temperature and the speed seems to vanish in both cases at the top boundary $z = 0$. This is sufficiently satisfying to make us consider the penalization method as a good one, thus we trust our future simulations, including phase change.

Still we need to zoom a bit in the damping zone to understand the role it has. On FIGURE 2.4, we see that the damped fields don't vanish exactly on $z = 0$ (the interface), they can only tend to 0 as we go further in the solid. This will have an impact on some of the next studies, so we should keep in mind that this penalization method implies a blurred interface that doesn't simply make the field vanishing at the exact analytic position $z = 0$.

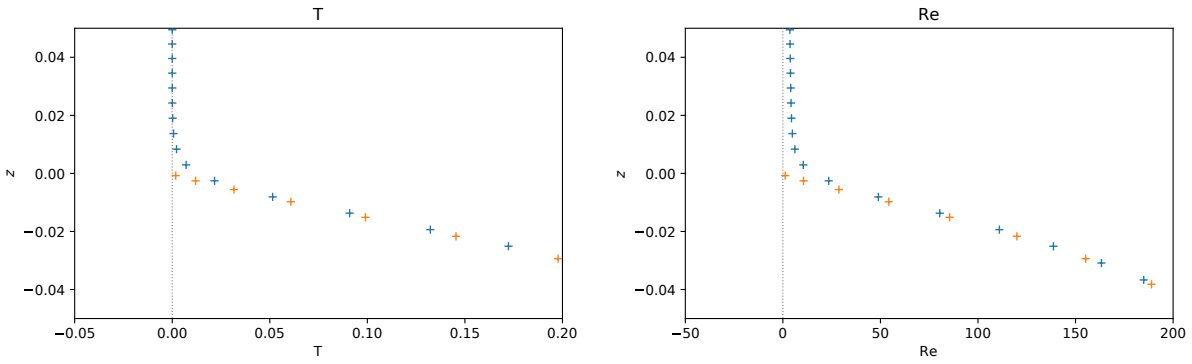

FIGURE 2.4 – Average profiles (along x and time) of the temperature (left) and the REYNOLDS number (right) in the real RAYLEIGH-BÉNARD problem (orange) and the damped problem (blue). The profiles have been zoomed around the interface.

3 The disk geometry

3.1 A cooling problem

Now we consider the following system : a disk of fluid with a certain temperature field $T \geq 0$ encircled by ice where $T \leq 0$. Everything is the same as previously, but still this induce a huge difference : we don't bring energy anymore to the system, the equivalent of the previous bottom border is now the center of the circle (higher temperature), but here we don't impose a fixed temperature. This implies that the energy will progressively leave the system and the mean temperature will decrease in time. Given that, we understand that the RAYLEIGH number will not be useful anymore : as it is defined with the temperature scale, we should define an **effective RAYLEIGH number** $\mathrm{Ra}_{\mathrm{eff}}$ that will follows the cooling process :

$$\mathrm{Ra}_{\mathrm{eff}}(t) = \mathrm{Ra}\frac{\langle T\rangle(t)}{\langle T\rangle(0)}$$

The same goes with the NUSSELT number. In the APPENDIX, we give an explanation of how we define it, but of course the goal is still to compare the leaving flux with the one in the diffusive case.

NB

$\langle\cdot\rangle_V$ now indicates a mean only over the liquid volume, the ice shouldn't be taken into account in this value :

$$\langle X\rangle = \frac{\langle \phi X\rangle_V}{\langle \phi\rangle_V}$$

Where $\langle\cdot\rangle_V$ is the total volume average.

3.2 Without melting

Before to consider the final system, we're trying to investigate some issues only due to the disk geometry. Thus we consider a static disk of fluid of radius $R = 1$. As in sub-section 2.2, we impose a

no-slip and fixed temperature at the boundary $R = 1$, thanks to the penalization method, so we keep the same set of equations 2.2.

$$\partial_t \langle T \rangle_V = - \left\langle \frac{\mathrm{Pr}}{\Gamma} (1 - \phi) T \right\rangle_V$$

NB

Here we can forget the difference between the averages $\langle \cdot \rangle$ and $\langle \cdot \rangle_V$, because the phase mask ϕ doesn't move in time and the temperature in the ice vanishes, so they only differ from a constant (cf. APPENDIX 4.4)

3.2.1 Cooling rate

Since the temperature decreases, it could be interesting to focus on the cooling rate. Without turbulence, we can derive a theoretical cooling rate : the solution of this diffusive problem has the following temperature distribution (see APPENDIX)

$$\overline{T}(r, t) = e^{-{x_0}^2 t} J_0(x_0 r)$$

Where J_0 is the BESSEL function of order 0 and x_0 is its first root. So here it is clear that the cooling rate is $\alpha = {x_0}^2 \sim 5.78$. This solution can be reached if the there is no convection, that is to say at low Ra. But for any value of Ra, there is no reason that the temperature decreases with that same rate. In particular we expect it to be higher, since turbulence allows the fluid in the center to go directly near, where the energy well $(1 - \phi)\, T$ is more effective.

On our simulations, we try to check these lasts properties. The FIGURE 3.1 shows how the temperature decreases in time. For a low initial RAYLEIGH number ($\mathrm{Ra} = 10^3$), the exponential decreasing is quickly verified, which means that we were close to the diffusive regime. For a higher Ra, it is clear that this exponential decreasing is reached later. On both simulations, the cooling rate is not exactly equal to ${x_0}^2 \sim 5.78$, this can be due to the fact that the exact field $\overline{T}(r, t)$ cannot be reached since we work with a penalization method and not on an exact boundary condition. In particular, as shown in sub-section 2.2, this numerical method is designed to mimic the physical solution everywhere except close the boundaries, in the damping zone, where of course the calculated fields, doesn't have anything physical. This implies that T will never exactly vanish at $r = 1$, and, because the cooling rate is directly linked with the size of the disk (cf. APPENDIX 4.5), this has a non trivial impact of its value. Since we don't have an other way of computation, we can still check that calculated cooling rate isn't that far from the theoretical one.

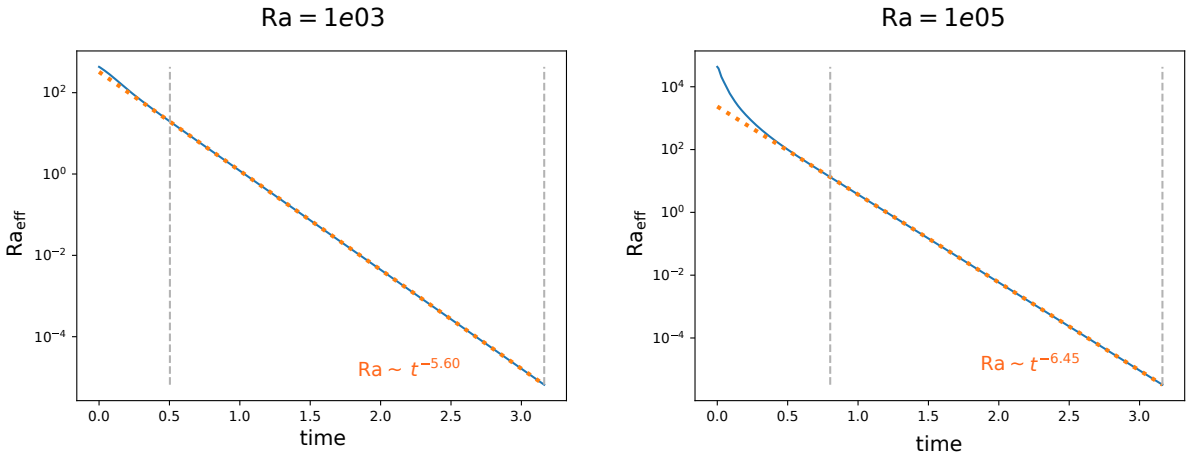

FIGURE 3.1 – The evolution of the effective RAYLEIGH number (proportional to $\langle T \rangle_V$) in time for two different initials Ra ($\mathrm{Ra} \in [10^3, 10^5]$). The vertical dotted lines are delimiting the time over which we compute the linear regression (orange).

3.2.2 Stability of the diffusive solution

After this decreasing temperature period, the system reach the stable diffusive solution :

$$\overline{T}(r,t) = e^{-{x_0}^2 t} J_0(x_0 r)$$

In the rectangular geometry, there were a diffusive solution $T_{lin} = -z$ which is supposed to be stable for $\mathrm{Ra} < 1710$. Here we can also look for such a critical RAYLEIGH number $\mathrm{Ra_c}$ at which the first instabilities start to grow. In order to do so, we will use the fact that this is a cooling process : the effective RAYLEIGH number will go down, until the diffusive regime in installed, for a certain value $\mathrm{Ra_c}$ of $\mathrm{Ra_{eff}}$. Thanks to some calculations (see APPENDIX), we are able to identify the beginning of this regime with the equation

$$\mathrm{Nu}(\mathrm{Ra_{eff}}) = \mathrm{cste}$$

We give on FIGURE 3.2 the evolution of Nu in function of $\mathrm{Ra_{eff}}$ during a simulation of an initial $\mathrm{Ra} = 10^5$. We see the establishment of the diffusive regime under $\mathrm{Ra_c}(\mathrm{Ra} = 10^5) \sim 10$. This value shouldn't change, given an other initial Ra. We didn't focus more on the exact value of $\mathrm{Ra_c}(\mathrm{Ra_{eff}})$, but on a range of $\mathrm{Ra} \in [10^2, 10^8]$, the critical value is pretty constant $\mathrm{Ra_c} \sim 10$. This is consistent with what we discussed in sub-section 3.2.1, where the linear evolution of $\mathrm{Ra_{eff}}$ in time seems to start at $\mathrm{Ra_{eff}} \sim 10$.

One can notice that this is far from the critical number $\mathrm{Ra_c} = 1710$ is the rectangular geometry... One explanation for this difference may be that here we have a dynamic problem, so some hysteresis phenomena can appear. In other words, we here estimate a critical RAYLEIGH number when the temperature decreases, which may not be the same as the one in the static case.

3.3 With melting

Here comes the final system we want to study... Let's suppose that we have an isotherm solid with a little circular cavity (initial radius R_i) of fluid in it. The temperature of the solid is uniform and equal to the melting temperature $T_m = 0$, and for the initial temperature field in the cavity, we take the diffusive solution. As we explained in APPENDIX 4.5, the initial cooling rate (as the diffusive profile is approximately maintained) increases as the radius decreases.

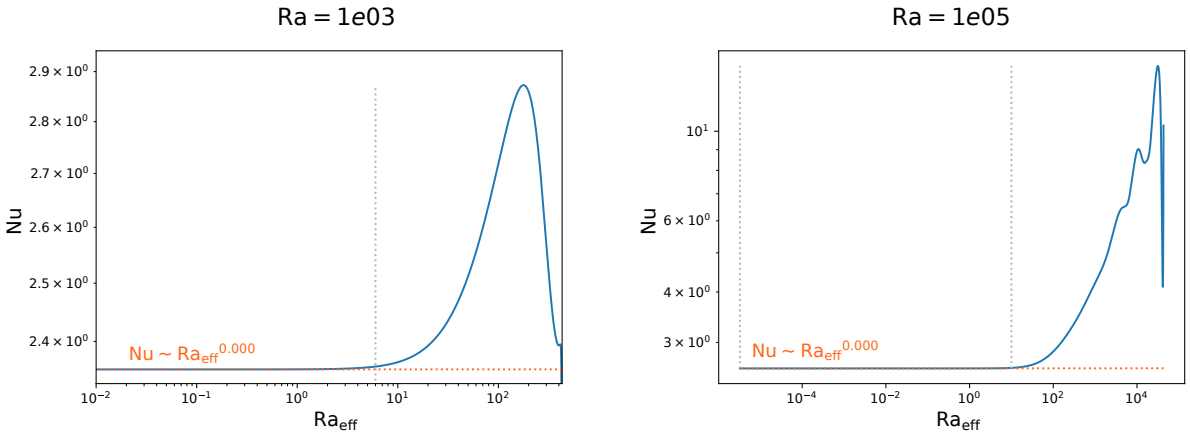

FIGURE 3.2 – Evolution of Nu with $\mathrm{Ra}_{\mathrm{eff}}$ for an initial $\mathrm{Ra} = 10^3, 10^5$. Nu seems to remain constant under $\mathrm{Ra}_{\mathrm{eff}} < \mathrm{Ra}_{\mathrm{c}} = 10$, which testify the establishment of the diffusive regime.

There is a snapshot of how it looks on FIGURE 4.1, but the problem wasn't exactly the same, since there were still a temperature gradient in the solid...

As we give some potential heat energy at the initial state (via the higher temperature in the cavity), we should only see the solid melt, until all this energy is consumed. So there should be an increase of the fluid's area, which can be calculated from the initial form of temperature T_i (cf. APPENDIX 4.8) :

$$\Delta S = \frac{1}{\mathrm{St}} \iint T_i \, \mathrm{d}S \tag{3.1}$$

And as explained in the APPENDIX 4.8, with an initial radius of $R = 1$ and the fixed initial temperature field $\overline{T}(0)$, then this integral can be calculated :

$$\Delta S = \frac{0.22}{\mathrm{St}} \tag{3.2}$$

On FIGURE 3.3 which shows preliminary simulations of the problem, it is clear that the effective RAYLEIGH number converge to a final value $T_f > 0$ which isn't consistent with the idea of a final state where the temperature of the fluid is zero. The surface S of the fluid on the other hand, also converge to a finite value (which was expected), but the given variation $\Delta S \sim 1$ is way higher than the expected value ($0.22/1 = 0.22$).

Conclusion

This internship was the very first step to a new type of studies, mixing turbulence and phase change. It was the occasion to implement the phase-field method on `dedalus`, so that we can get some clues about the numerical context, as well as the physical one. We started to see how the heat flux behaves, relatively to the turbulence on a simple geometry, then we included some phase-change and we modified the geometry, in order to see, at each step, the influence of the new physical ingredient. Finally, we didn't have much time to focus on the final system, which was the goal at the beginning. But the different problems we encountered allowed us to go deeper on some specific issues (numerical and physical ones), that we couldn't anticipate. This internship is now supposed to lay the foundations for the next studies on this specific subject, that will soon push forward our understanding of the dynamics of subglacial liquid environments.

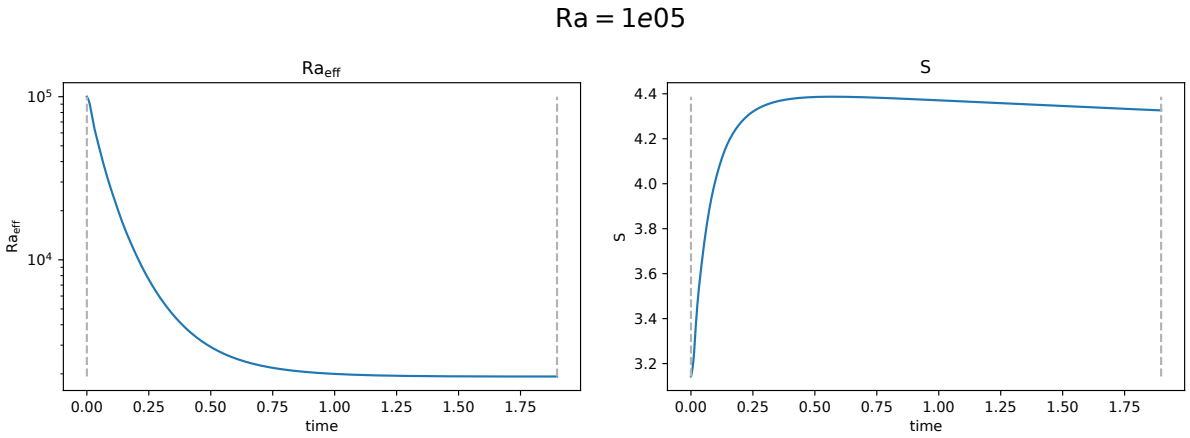

FIGURE 3.3 – Evolution of the effective RAYLEIGH number and the surface S of the fluid in time, for an initial $\mathrm{Ra} = 10^5$ and $\mathrm{St} = 1.0$... It seems that both of them converge to a final value.

4 Appendix

4.1 Non-dimensionalisation of the NAVIER-STOCKES equations

It is useful to notice that the gravitational term can be rewritten as follows :

$$\begin{aligned}
\delta\rho\,\boldsymbol{g} &= \rho_0\beta(T - T_0)\,\boldsymbol{e_z} \\
\delta\rho\,\boldsymbol{g} &= \rho_0\beta\left(\Delta T\left(\tilde{T} + \frac{z}{h}\right) - T_0\right)\boldsymbol{e_z} \\
\delta\rho\,\boldsymbol{g} &= \rho_0\Delta T\left(\beta\tilde{T}\right)\boldsymbol{e_z} + \rho_0\beta\,\boldsymbol{\nabla}\left(\frac{\Delta T}{2h}z^2 - T_0 z\right)
\end{aligned}$$

On can then redefine the pressure, in order to include the second term in it :

$$p = P - \rho_0\beta\left(\frac{\Delta T}{2h}z^2 - T_0 z\right) \qquad \text{then} \quad \tilde{p} = \frac{h^2}{\rho_0\kappa^2}\,p$$

Likewise we can explicit the term of heat's convection :

$$\boldsymbol{u}\cdot\boldsymbol{\nabla}T = \frac{\kappa\Delta T}{h^2}\,\tilde{\boldsymbol{u}}\cdot\tilde{\boldsymbol{\nabla}}(\tilde{T} + \tilde{z}) = \frac{\kappa\Delta T}{h^2}\,(\tilde{\boldsymbol{u}}\cdot\tilde{\boldsymbol{\nabla}}\tilde{T} + \tilde{w})$$

4.2 Properties of the NUSSELT number

Here we consider the dimensional quantities. The heat equation is

$$\rho_0 c_p\left(\partial_t T + \boldsymbol{u}\cdot\boldsymbol{\nabla}T\right) = \lambda\nabla^2 T$$

With λ the thermal conductivity of the fluid, c_p its thermal capacity and ρ_0 its density. As a recall, the thermal diffusive coefficient is given by $\kappa = \frac{\lambda}{\rho_0 c_p}$. We can then extract the heat flux $\boldsymbol{j}$:

$$\rho_0 c_p\partial_t T + \operatorname{div}\underbrace{\left(\rho_0 c_p T\boldsymbol{u} - \lambda\boldsymbol{\nabla}T\right)}_{\boldsymbol{j}} = 0 \qquad \text{since} \quad \boldsymbol{\nabla}\cdot\boldsymbol{u} = 0$$

Then we non-dimensionalize this flux

$$\boldsymbol{j} = \frac{\lambda\,\Delta T}{h}\underbrace{\left((\tilde{T} - \tilde{z})\tilde{\boldsymbol{u}} - \tilde{\boldsymbol{\nabla}}(\tilde{T} - \tilde{z})\right)}_{\tilde{\boldsymbol{j}}}$$

Now all the quantities are considered non-dimensionalized and we forgot the $\tilde{}$, so that we separate the flux into two terms :

$$\begin{aligned} q &= \boldsymbol{j} \cdot \boldsymbol{e_z} \\ q &= (T-z)w - \partial_z(T-z) \\ q &= \underbrace{(T-z)w}_{q_{conv}} + \underbrace{(1-\partial_z T)}_{q_{diff}} \end{aligned}$$

But we will always compute the mean over x of those quantities, so it is useful to notice that simplification :

$$\begin{aligned} \langle zw \rangle_x &= z \langle w \rangle_x \\ \langle zw \rangle_x &= \frac{z}{\gamma} \int_0^\gamma w \, \mathrm{d}x \end{aligned}$$

Yet the fluid is incompressible :

$$\begin{aligned} 0 &= \partial_x u + \partial_z w \\ \implies 0 &= \int_0^z \mathrm{d}z' \partial_x u + [w]_0^z \qquad \text{avec} \quad w(z=0) = 0 \\ \implies 0 &= \int_0^\gamma \mathrm{d}x \int_0^z \partial_x u + \int_0^\gamma w \, \mathrm{d}x \\ \implies \int_0^\gamma w \, \mathrm{d}x &= -\int_0^z \mathrm{d}z \int_0^\gamma \partial_x u \, \mathrm{d}x \\ \implies \int_0^\gamma w \, \mathrm{d}x &= -\int_0^z \mathrm{d}z [u]_0^\gamma \qquad \text{avec} \quad u(x=0) = u(x=\gamma) 0 \\ \implies \int_0^\gamma w \, \mathrm{d}x &= 0 \end{aligned}$$

Thus we have

$$\langle zw \rangle_x = 0 \implies \langle q_{conv} \rangle_x = \langle Tw \rangle_x$$

Likewise it exists a simplification on the diffusive part of the flux when we calculate the vertical average :

$$\begin{aligned} \langle q_{diff} \rangle_z &= \int_0^1 (1 - \partial_z T) \\ \langle q_{diff} \rangle_z &= 1 - [T]_{z=0}^{z=1} \\ \langle q_{diff} \rangle_z &= 1 \end{aligned}$$

From the last considerations, we derive the following properties for the Nusselt number :

$$\begin{aligned} \mathrm{Nu} &= 1 + (T-z)w - \partial_z T \\ \langle \mathrm{Nu} \rangle_x &= 1 + \langle Tw \rangle_x - \langle \partial_z T \rangle_x \\ \langle \mathrm{Nu} \rangle_V &= 1 + \langle Tw \rangle_V \end{aligned}$$

Finally we can prove a last interesting property... Let's go back to the heat equation

$$\partial_t T + \boldsymbol{\nabla} \cdot \boldsymbol{j} = 0$$

With $\boldsymbol{j} = j_x \boldsymbol{e_x} + \mathrm{Nu}\boldsymbol{e_z}$. Once the final permanent regime is reached, we can compute the time average to get this :

$$\begin{aligned} 0 &= \overline{\partial_t T} = \partial_t \overline{T} \\ \implies 0 &= \partial_x \overline{j_x} + \partial_z \overline{\mathrm{Nu}} \end{aligned}$$

Then we take the horizontal average, in which the first term vanishes thanks to the periodicity

$$\langle \partial_x j_x \rangle_x = \frac{1}{\gamma} \int_0^\gamma j_x \, \mathrm{d}x = \frac{1}{\gamma} [j_x]_0^\gamma = 0$$

Thus we have

$$\partial_z \langle \overline{\mathrm{Nu}} \rangle_x = 0 \implies \langle \overline{\mathrm{Nu}} \rangle_x = \mathrm{cste}$$

4.3 Influence of the last term in the melting equations

Let's remind us the equation of phase change :

$$\frac{5}{6}\mathrm{St}\, \partial_t \phi = \nabla^2 \phi + \underbrace{\frac{16}{\delta^2}\, \phi(1-\phi)(2\phi - 1 + T)}_{Q}$$

In order to have a better understanding of the last term $Q = {}^{16}/_{\delta^2}\, \phi(1-\phi)(2\phi-1+T)$, let's just illustrate it on a simple example : a cavity with an initial shape of disk. On FIGURE 4.1, we see that Q is close to zero everywhere except on the interface (thanks to $\phi(1-\phi)$), so it will only affect the boundary. But on the interface, it is positive in the fluid side and negative in the solid side, this is due to $2\phi - 1 + T$ which change its sign on the middle of the interface, where $\phi \sim {}^1/_2$ and $T \sim 0$.

In the fluid side, right before the interface $\phi \sim 1$ but this term make it increase even more ($Q > 0$), it is supposed to balance the diffusive term $\nabla^2 \phi$, which tends to make the interface become wider, and homogenise the system. The parameters ${}^5/_6\mathrm{St}$ and ${}^{16}/_{\delta^2}$ are chosen so that the non-linearities exactly balance the diffusion, in order to keep a very small damping-zone, that follows the theoretical interface.

4.4 Equivalence between two averages in the non melting case

In the case of a static solid phase, the average over the whole volume $\langle \cdot \rangle_V$ is proportional to the average over the fluid phase $\langle \cdot \rangle$. Let L^2 be the area of the total volume, S the one of the fluid cavity and X a field that vanishes in the solid because of a damping term (temperature or speed).

$$\begin{aligned} \langle X \rangle_V &= \frac{1}{L^2} \iint_V X \mathrm{d}x\mathrm{d}z \\ \langle X \rangle_V &= \frac{1}{L^2} \left(\iint_{\text{liquid}} X \, \mathrm{d}x\mathrm{d}z + \iint_{\text{ice}} X \, \mathrm{d}x\mathrm{d}z \right) \\ \langle X \rangle_V &\sim \frac{1}{L^2} \iint_{\text{liquid}} X \, \mathrm{d}x\mathrm{d}z \\ \langle X \rangle_V &\sim \frac{S}{L^2} \langle X \rangle \end{aligned}$$

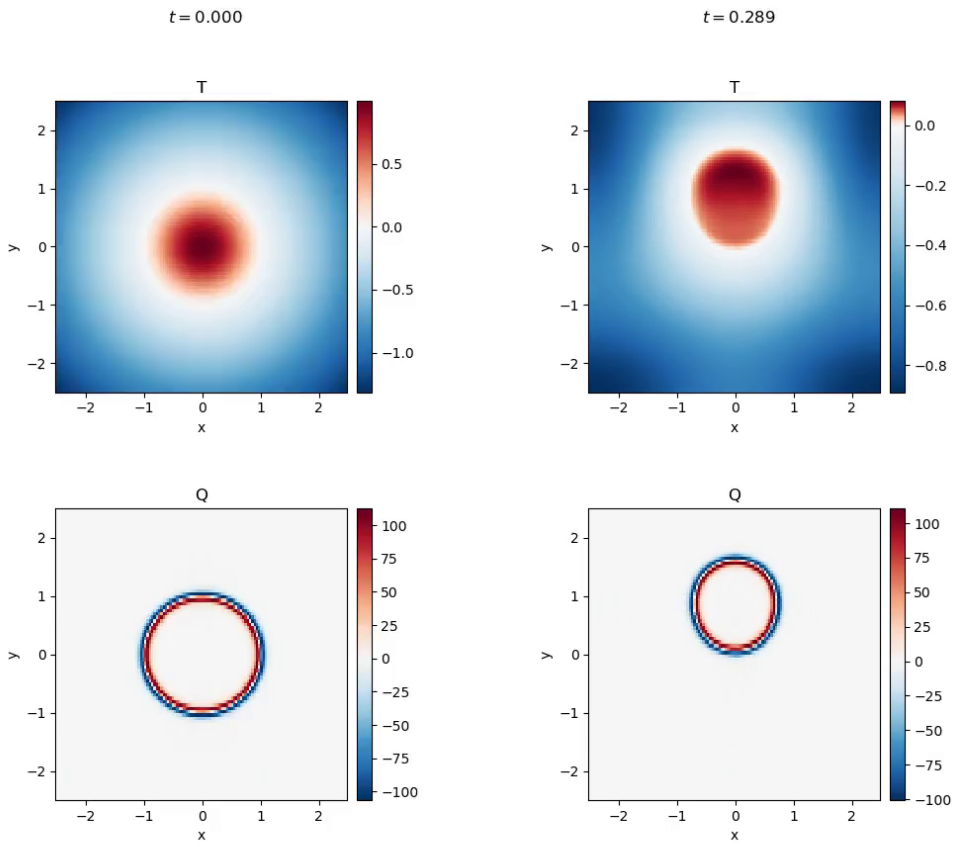

FIGURE 4.1 – The shape of the fields T and Q at two different moments.

Indeed, the average of X in the fluid of area S is

$$\langle X \rangle = \frac{1}{S} \iint_{\text{liquid}} X \, \mathrm{d}x\mathrm{d}z$$

4.5 Diffusive solution on the disk geometry without melting

We're trying to find the analytical solution of the temperature field for the heat equation without the convective term :

$$\partial_t \overline{T} = \Delta \overline{T}$$

Let's suppose that the solution will be a stationary field, with a symmetry of rotation (the dependence with θ) :

$$\overline{T}(r,t) = f(t)g(r) \implies \frac{f'}{f} = \frac{\Delta g}{g} = -\alpha < 0$$

The constant α has to be negative, so that $f(t) = e^{-\alpha t}$ will decrease and the total energy falls down instead of growing up. The solution for the equation of g is the first BESSEL function $g(r) = J_0(\sqrt{\alpha} r)$. Let $x_0 \sim 2.40$ be the first root of J_0, we want the temperature to vanish at $r = 1$, so we need to have $\sqrt{\alpha} = x_0$, so that the final solution is (assuming an initial temperature $\overline{T}(0,0) = 1$ at the center)

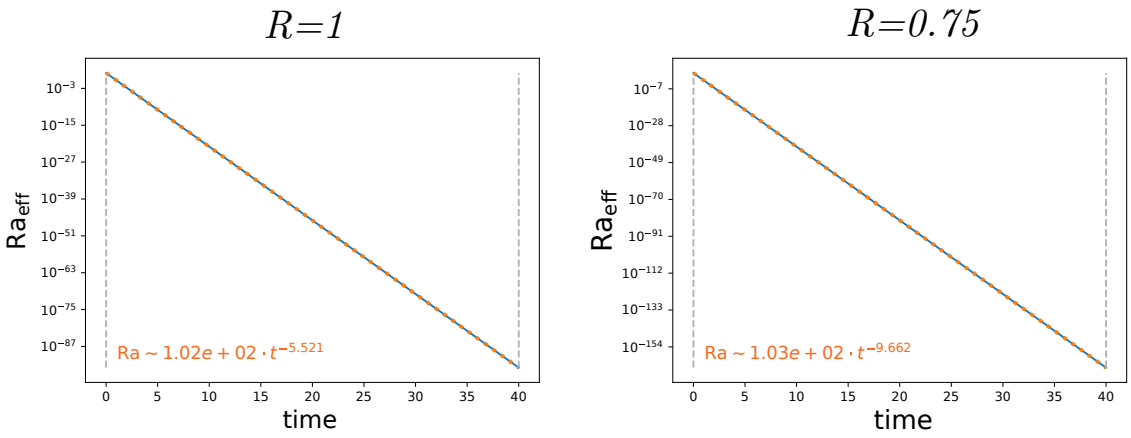

FIGURE 4.2 – The evolution of the temperature in the diffusive regime ($\mathrm{Ra} = 10^2$) for two different radius ($R = 1$ and $R = 0.75$). It appears that the cooling process is faster when the radius decreases.

$$\overline{T}(r,t) = e^{-{x_0}^2 t} J_0(x_0 r)$$

In particular the cooling rate is fixed at ${x_0}^2 \sim 5.78$, this is a verified in our simulations. We can still notice that in a general case, with a cavity of radius R, the solution is

$$\overline{T}(r,t) = e^{-(x_0/R)^2 t} J_0\left(\frac{x_0}{R} r\right) \tag{4.1}$$

So the cooling rate is directly linked with the radius R, in particular the smaller the cavity is, the faster the system cools off. This clearly appears on the simulations (cf. FIGURE 4.2). This can be an explanation, for the gap between the observed cooling rate and the theoretical one (cf. subsection 3.2.1).

4.6 Evolution of the NUSSELT number with the effective RAYLEIGH number in the diffusive regime on the disk geometry without melting

In order to define a NUSSELT number, we need to consider the outer flux $q = \boldsymbol{j} \cdot \boldsymbol{e_r}$ that leaves the disk, so we integrate it on a the circle $r = 1$ to get the mean

$$\langle q \rangle_\theta (r = 1) = \frac{1}{2\pi} \oint q \, \mathrm{d}\theta$$

With the damping term

In case of the damping method, we have

$$\partial_t \langle T \rangle_V = - \left\langle \frac{\mathrm{Pr}}{\Gamma} (1 - \phi) T \right\rangle_V$$

instead of

$$\begin{aligned} \partial_t T &= -\mathrm{div}\, \boldsymbol{j} \\ \partial_t \langle T \rangle_V &= -\frac{1}{\pi} \oint q \, \mathrm{d}\theta \\ \partial_t \langle T \rangle_V &= -2 \langle q \rangle_\theta (r = 1) \end{aligned}$$

So we identify

$$Q_{out} = 2\langle q\rangle_\theta(r=1) = \left\langle \frac{\mathrm{Pr}}{\Gamma}(1-\phi)T \right\rangle_V$$

The Nusselt number compares this flux with the one in the diffusive case :

$$\overline{q} = -\partial_r \overline{T} = -x_0 e^{-{x_0}^2 t} J_0'(x_0 r) \implies \langle \overline{q}\rangle_\theta(r=1) = -x_0 e^{-{x_0}^2 t} J_0'(x_0)$$

Here comes a tricky part : $\overline{q}$ decrease exponentially in time, assuming that the diffusive regime in reached from the beginning. But the system can start to show some turbulence, before its temperature is sufficiently low to follow the diffusive regime. We don't know when this is supposed to arrive, so the time dependent factor will be redefined, so that the time t is shifted to fit with the actual $\mathrm{Ra_e ff}$:

$$\langle \overline{q}\rangle_\theta(r=1) = -x_0 \frac{\mathrm{Ra_{eff}}}{\mathrm{Ra}} J_0'(x_0)$$

So that the Nusselt number is

$$\mathrm{Nu} = \frac{\langle q\rangle_\theta(r=1)}{\langle \overline{q}\rangle_\theta(r=1)} = -\frac{Q_{out}}{x_0 J_0'(x_0)} \frac{\mathrm{Ra}}{\mathrm{Ra_{eff}}}$$

Now the point is the to get the evolution of Nu with $\mathrm{Ra_{eff}}$ in the diffusive regime :

$$\partial_t \langle \overline{T}\rangle_V = -Q_{out}$$
$$-{x_0}^2 \langle \overline{T}\rangle_V = -Q_{out}$$

Then, with the previous definition of Nu, we see that

$$\mathrm{Nu} \propto \frac{Q_{out}}{\langle \overline{T}\rangle_V}$$

Combined with the last equation, we get

$$\mathrm{Nu} = \mathrm{cste}$$

4.7 Definition of the Nusselt number in the case of a melting disk

In the last sub-section, we tried to define a Nusselt number Nu, that still compares the flux that leaves the system to the one in a purely diffusive regime. It was a bit tricky because the temperature were varying, so the diffusive flux $\overline{q}$ had to be rescaled, by replacing the exponential term with $^{\mathrm{Ra_{eff}}}/_{\mathrm{Ra}}$. We now want to generalize it to the next step : we reintroduce the possibility of phase change. There are two new problems :

1. The leaving flux is not calculated by the damping term anymore $\left\langle \frac{\mathrm{Pr}}{\Gamma}(1-\phi)T \right\rangle_V$
2. The shape of the cavity is now changing, so the diffusive solution doesn't keep its analytical solution

The first point is not a big deal, since the calculations are the same as before :

$$\partial_t \langle T\rangle_V = -\mathrm{St}\, \partial_t \langle \phi\rangle_V$$

So the equivalent of Q_{out} is now

$$Q_{out} = \mathrm{St}\,\partial_t\langle\phi\rangle_V = \frac{\mathrm{St}}{L^2}\iint \phi\,\mathrm{d}S$$

The second problem is a bit different and we'll need to do some approximations... Since $\overline{q}$ must be calculated analytically, we need to suppose a certain shape for the cavity. Of course, we'll suppose that it keeps its disk shape with a varying radius $R(t)$. We can get this equivalent radius from the area of the liquid phase :

$$S = \iint \phi\,\mathrm{d}S \equiv \pi R^2 \implies R = \sqrt{\frac{S}{\pi}}$$

Then with equation 4.1, we can get a diffusive solution, in which we replace the exponential decreasing term by $\mathrm{Ra}_{\mathrm{eff}}/\mathrm{Ra}$, since we have a cooling process :

$$\overline{T} = \frac{\mathrm{Ra}_{\mathrm{eff}}}{\mathrm{Ra}}\,J_0\left(\frac{x_0}{R}r\right)$$

Thus the leaving flux of that equivalent disk is

$$\langle\overline{q}\rangle_\theta(r=R) = -\frac{x_0}{R}\frac{\mathrm{Ra}_{\mathrm{eff}}}{\mathrm{Ra}}\,J_0'(x_0)$$

So that the final definition for Nu is

$$\mathrm{Nu} = -\frac{\mathrm{RaSt}}{L^2 x_0 J_0'(x_0)}\,\frac{R\partial_t S}{\mathrm{Ra}_{\mathrm{eff}}} = -\frac{\mathrm{RaSt}}{\sqrt{\pi}L^2 x_0 J_0'(x_0)}\,\frac{\sqrt{S}\partial_t S}{\mathrm{Ra}_{\mathrm{eff}}}$$

4.8 Spreading of the fluid inside an isotherm solid at the melting temperature

The initial state is simple : we consider an infinite uniform solid at the melting temperature $T_m = 0$. There is a cavity of fluid with a shape of a disk of initial radius R_i. Let $T_i(r,\theta) > 0$ be the initial temperature field in it. So that the total temperature field (liquid + solid) is

$$T_i(r,\theta) = \Theta(R_i - r)T_i(r,\theta)$$

Where $\Theta(x)$ is the HEAVISIDE function

$$\Theta(x) = \begin{cases} 1 & \text{if} \quad x \geq 0 \\ 0 & \text{if} \quad x < 0 \end{cases}$$

Choosing this initial state fix the total accessible energy, that is to say the extractible energy from the fluid when its temperature falls down to $T_m = 0$:

$$E = \iint (T_i - T_m)\,\rho c_p\,\mathrm{d}S = \rho c_p \iint T_i\,\mathrm{d}S$$

When the final state is reached, there shouldn't be any flux nor in the fluid, nor in the solid. So both of them have to be at a the same temperature : $T_m = 0$ (cf. FIGURE 4.3). So all of the previously defined accessible energy in used to make the solid melt :

$$E = \mathcal{L}\rho\,\Delta S$$

Where $\mathcal{L}$ is the latent heat and ΔS is the variation of the fluid's area during the melting process... Combining the two previous equations, we get **in terms of non-dimensionalized quantities** :

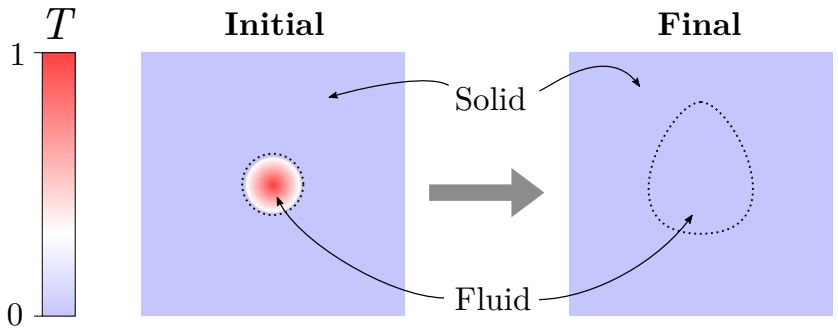

FIGURE 4.3 – At the initial state, only a disk of fluid is at a temperature higher than $T_m = 0$. All the energy contained in the fluid, will be absorbed by the phase change, until the whole system is at equilibrium, which implies a single temperature $T_m = 0$.

St	R_f
1	1.20
0.5	1.37
0.1	2.31

TABLE 2 – Some of the final radius in function for different values of St at a fixed initial radius $R_i = 1.00$

$$\Delta S = \frac{1}{\mathrm{St}} \iint T_i \, \mathrm{d}S$$

We can have a better understanding of this relation, considering a given initial state. In our simulations, we always start from the diffusive solution

$$T_i(r, \theta) = J_0\left(\frac{x_0}{R_i} r\right)$$

And we can estimate

$$\int_0^{R_i} J_0\left(\frac{x_0}{R_i} r\right) r \, \mathrm{d}r = \left(\frac{R_i}{x_0}\right)^2 \int_0^{x_0} J_0(u) u \, \mathrm{d}u \sim 0.22 \, {R_i}^2$$

So that

$$\Delta S \sim \frac{2\pi \cdot 0.22 \, {R_i}^2}{\mathrm{St}}$$

To have on other order of magnitude, let's suppose that the cavity maintain its disk geometry from a radius R_i to R_f :

$$\Delta S = \pi \left({R_f}^2 - {R_i}^2\right)$$
$$R_f = \sqrt{{R_i}^2 + \frac{0.43 \, {R_i}^2}{\mathrm{St}}} = R_i \sqrt{1 + \frac{0.43}{\mathrm{St}}}$$

Let's assume that we start with an initial radius $R_i = 1$, we give some of the final radius in function of St on the TABLE 2.

References

[1] Hendrix et al. The NASA Roadmap to Ocean Worlds. Astrobiology, 19(1) :1–27, January 2019.

[2] Planetary Decadal Survey - White Paper Proposals.

[3] Scully et al. The varied sources of faculae-forming brines in Ceres' Occator crater emplaced via hydrothermal brine effusion. Nature Communications, 11, August 2020.

[4] Kalousová et al. Water generation and transport below Europa's strike-slip faults : Water generation below Europa's faults. Journal of Geophysical Research : Planets, 121(12) :2444–2462, December 2016.

[5] E. Lesage, H. Masssol, and F. Schmidt. Cryomagma ascent on Jupiter's moon Europa. page 2, 2020.

[6] C. Málaga, F. Mandujano, R. Peralta-Fabi, and C. Arzate. Non-Boussinesq rolls in 2d thermal convection. European Journal of Mechanics - B/Fluids, 49 :65–70, January 2015.

[7] Hao Song, E. Villermaux, and Penger Tong. Coherent oscillations of turbulent Rayleigh-Bénard convection in a thin vertical disk. Physical Review Letters, 106(18) :184504, May 2011.

[8] Louis-Alexandre Couston, Eric Hester, Benjamin Favier, John R. Taylor, Paul R. Holland, and Adrian Jenkins. Topography generation by melting and freezing in a turbulent shear flow. Journal of Fluid Mechanics, 911, March 2021. Publisher : Cambridge University Press.

[9] E. Hester, L.-A. Couston, B. Favier, K. Burns, and G. Vasil. Improved phase-field models of melting and dissolution in multi-component flows | Proceedings of the Royal Society A : Mathematical, Physical and Engineering Sciences, 2020.

[10] Keaton J. Burns, Geoffrey M. Vasil, Jeffrey S. Oishi, Daniel Lecoanet, and Benjamin P. Brown. Dedalus : A flexible framework for numerical simulations with spectral methods. Physical Review Research, 2(2) :023068, April 2020. Publisher : American Physical Society.

[11] Siegfried Grossmann and Detlef Lohse. Scaling in thermal convection : a unifying theory. Journal of Fluid Mechanics, 407 :27–56, March 2000.

[12] E. M. King, S. Stellmach, and J. M. Aurnou. Heat transfer by rapidly rotating Rayleigh–Bénard convection. Journal of Fluid Mechanics, 691 :568–582, January 2012. Publisher : Cambridge University Press.